J. Fluid Mech. (1991), *vol.* 227, *pp.* 543–566
Printed in Great Britain

Horizontal jets and vortex dipoles in a stratified fluid

By S. I. VOROPAYEV, YA. D. AFANASYEV AND I. A. FILIPPOV

Institute of Oceanology, USSR Academy of Sciences, Krasikova 23, Moscow 117218, USSR

(Received 23 August 1988 and in revised form 4 December 1990)

When a horizontal force is applied locally to some volume of a viscous density-stratified fluid, flows with high concentration of vertically oriented vorticity (vortex dipoles) are generated. The processes of generation and evolution with time of these unsteady flows in a stratified fluid are studied. A convenient way to produce and study these flows in the laboratory is to use a submerged horizontal jet as a 'point' source of momentum. The main governing parameter (the 'force') is easily controlled in this case. Two regimes were studied: starting jets with dipolar vortex fronts (the force acts continuously) and impulsive vortex dipoles (the force acts for a short period of time). A conductivity microprobe, aluminium powder, shadowgraph, thymol-blue and other techniques have been used to measure the velocity and density distributions in the flows. It is found that in both regimes the flows are self-similar: the lengthscale of the flows increases with time as $t^{\frac{1}{2}}$ for starting jets and as $t^{\frac{1}{3}}$ for vortex dipoles. Detailed information about the generation mechanism, kinematics and dynamics of the flows is obtained. On the basis of similarity principles a theoretical explanation of the experimental results is given. The theory is in good agreement with the results obtained.

1. Introduction and summary

Axisymmetric vortex structures in a homogeneous fluid are a well-known phenomenon. They are easily formed in a viscous fluid when a force is applied locally to some volume of fluid. If a force acts for a short period of time, vortex rings are produced (see for example Batchelor 1967, photos 7.2.2 and 7.2.3). If the force acts continuously, a starting jet with a spherical vortex at its leading edge is generated (figure 1). Eventually this vortex travels away from the origin, forming a steady axisymmetric jet behind it. The steady axisymmetric jet in a homogeneous fluid was studied theoretically by Slezkin (1934), Landau (1944) and Squire (1951).

The vortex dipole, a flat analogue of a vortex ring, is easily formed in a stratified fluid, where the vertical motion is suppressed by the force of gravity (figure 2). In general, it is not important what kind of physical mechanism suppresses the motion perpendicular to the direction of the applied force and makes the flow quasi-two-dimensional. It can be the force of gravity in a stratified fluid (Voropayev 1983, 1987; van Heijst & Flor 1989), the Coriolis force in a rotating homogeneous fluid (Flierl, Stern & Whitehead 1983), the force of surface tension in a soap film (Couder & Basdevant 1986), or a magnetic field in a layer of mercury (Papaliou 1985; Nguyen Duc & Sommeria 1988). In all these cases vortex dipoles are formed easily. They are stable, have a long lifetime and are not destroyed in symmetric collisions (Couder & Basdevant 1986; Afanasyev, Voropayev & Filippov 1988; van Heijst 1989;

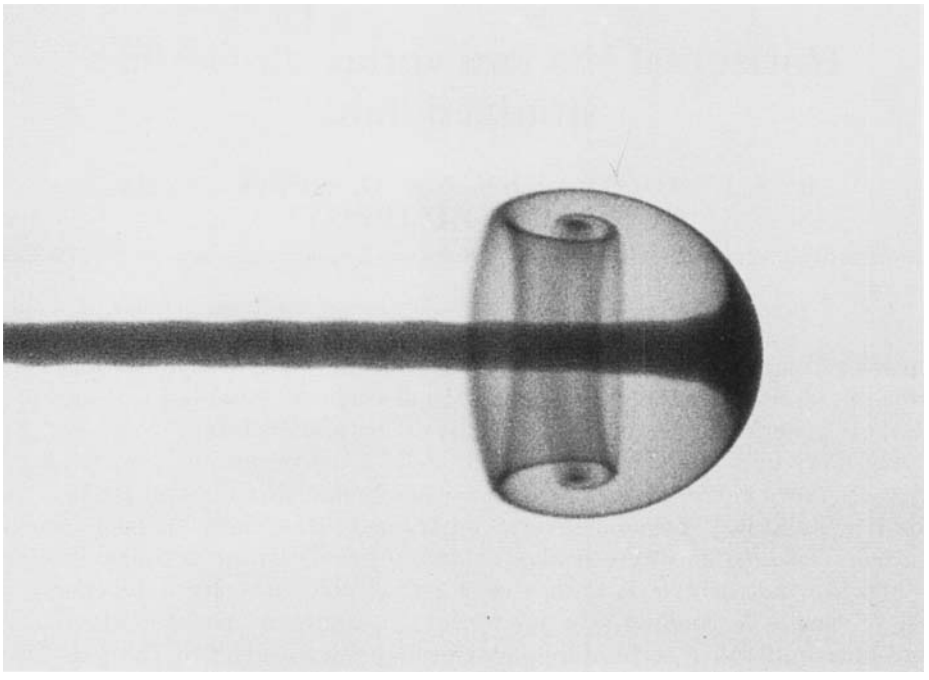

FIGURE 1. Dyed starting jet in a homogeneous fluid at $Re = 55$ (Voropayev 1985).

(a)

(b)

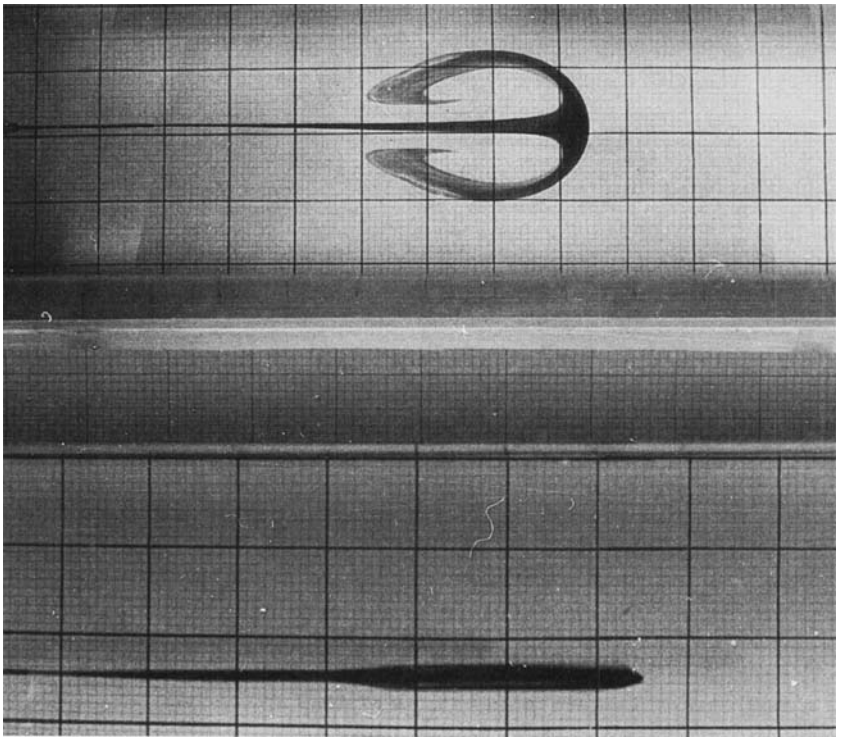

FIGURE 2. Dyed starting horizontal jet in a stratified fluid: (a) top view, (b) side view. $Re = 85$, $N = 1.2\ \mathrm{s}^{-1}$, grid in in. (Voropayev 1983).

Voropayev, Filippov & Afanasyev 1989). This type of collision has been described in detail in numerical simulations by McWilliams & Zabusky (1982) and McWilliams (1984). These authors also give an explanation in terms of solitons passing through each other. It seems that vortex dipoles and various forms of more complicated vortex structures are the universal product of any irregular forcing in two-dimensional systems. (See for example the results of numerical calculations of two-dimensional turbulence by McWilliams 1984.)

In recent years vortex dipoles, or mushroom-like currents (the name proposed by Ginsburg & Fedorov 1984 for these structures in the ocean), have become the subject of renewed interest, when they were discovered in great number on the visual and infrared satellite images of the upper ocean (for example, Ahlnäs, Royer & George 1987 determined 17 vortex dipoles on only one of their images).

Two types of solutions for steady non-viscous vortex dipoles are known. The first one is a 'non-compact' dipole consisting of two point vortices of opposite sign – a steady solution of the Euler equation. The second one is a compact couple in which the vorticity is proportional to the stream function inside the couple and vanishes outside (Lamb 1932). Symmetrical and also asymmetrical compact vortex couples have been studied experimentally and theoretically by Flierl *et al.* (1983) and Nguyen Duc & Sommeria (1988).

The main aim of our research was to consider unsteady viscous vortex dipole dynamics in a stratified fluid. It appears that consideration of submerged horizontal jet flow is needed for this purpose. Now we understand that jets and vortex dipoles are united by the same mechanism of generation – the action of a localized source of momentum in a viscous fluid.

In our experiments a jet from a thin round nozzle (diameter D) was used as a 'point' source of momentum. The jet was injected horizontally into a stratified fluid at the level of its equilibrium density (ρ). If the mean velocity at the nozzle exit is U_*, the mass flux is proportional to $Q_* \sim \rho D^2 U_*$ and the momentum flux is $J_* \sim \rho D^2 U_*^2 \sim Q_*^2/\rho D^2$ (in experiments $J_* = 4Q_*^2/\pi D_\rho^2$ is calculated from measured Q_*). Because of the viscous entrainment of ambient fluid, the total mass flux $Q(x)$ in the jet, which forms after the source has been turned on, increases rapidly with a distance x from the origin: $Q(x) \sim \nu\rho x$ (ν is the kinematic viscosity). In the experiments Q_* is so small that it soon becomes negligible compared to Q. Decreasing D and increasing U_* so that $J_* = \text{const.}$ we obtain a 'point' source of momentum exclusively which exerts a force J_*/ρ per unit mass on the fluid.

The results of the laboratory experiments and a theoretical explanation for them are given below. The following items are considered in this paper:

(i) A steady horizontal jet in a stratified fluid: self-similar distributions of experimentally measured velocities (§2.1).

(ii) A starting horizontal jet in a stratified fluid: theoretical explanation for our previous experimental results (Voropayev & Filippov 1985) and some new experimental data on the frontal vortex dipole and its characteristics (§2.2).

(iii) Experimental verification of the asymptotic solution of the two-dimensional Navier–Stokes equation for the low-Reynolds-number unsteady flow induced by a point force: a model of vortex dipole generation (§2.3).

(iv) An impulsive vortex dipole in a stratified fluid: experimental data and a theoretical explanation of experimental results (§3.1); Turner's model of the entrainment into an expanding vortex dipole (§3.2).

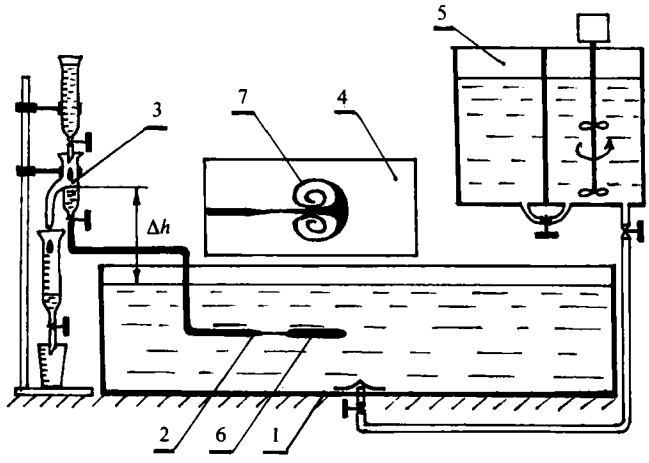

FIGURE 3. Sketch of experimental apparatus: 1, experimental tank with a stratified fluid; 2, horizontal nozzle; 3, water supply system with a constant-level bottle (Δh = const.); 4, 45° mirror; 5, two-tank system (left tank – salt water, right tank – fresh water); 6, side view of jet flow; 7, top view of jet flow.

1.1. *Experimental apparatus*

The experiments with starting and steady jets were conducted in a transparent rectangular tank $160 \times 40 \times 20$ cm (figure 3). A square tank $80 \times 80 \times 30$ cm was used in the experiments on impulsive vortex dipoles. Density stratification of the working fluid (distilled water) was created by variation of its salinity in the vertical direction. A linear vertical density distribution was produced using the well-known two-tank method. The density distributions were controlled by a single electrode (platinum) conductivity probe (Afanasyev, Voropayev & Filippov 1990). The flow in the tank was generated by a horizontal jet from a thin round nozzle (nozzle diameters D = 0.08–0.2 cm). To produce a constant volume flux through the nozzle we used a constant-level bottle (see 3 in figure 3). The main part of the experimental data discussed in this paper was obtained as a result of an analysis of motion pictures of the flows. For visualization of the flow we used a pH-indicator thymol-blue (Stern & Voropayev 1984), aluminium powder and the Schlieren technique. Longitudinal velocity distributions across the jet were measured using the thymol-blue technique proposed by Baker (1966). In these experiments were used pure saccharose to change the density of distilled water and to produce a linearly stratified fluid (salt increases significantly the conductivity of the solution and is not acceptable here). A cross of two fine platinum wires (diameter 2×10^{-3} cm, length 10 cm) was inserted into a jet axis (x-axis; the origin is at $x = 0$). One wire was vertical (along the z-axis) and the other was horizontal (along the y-axis). An a.c. voltage with low frequency (1–3 Hz) was applied to the wires. In a weak thymol-blue solution small cylinders of coloured fluid form regularly around the wires and move away, making neutrally buoyant markers. A mirror was used to take simultaneous top and side photographs. The vertical and horizontal distributions of longitudinal velocity U were calculated from voltage frequency and marker-displacement data at different distances x from the origin.

In some experiments (§2.3) two-layer stratification was used: a thin upper layer ($h \approx 0.4$ cm) of a light viscous fluid (aqueous glycerin, $\nu = 2.7 \times 10^{-2}$ cm^2 s^{-1}) lying on a thick layer of a heavy low-viscosity fluid (CCl_4, $\nu_* = 0.5 \times 10^{-2}$ cm^2 s^{-1}). The low-

Reynolds-number flow was generated only in the upper layer by the slitted nozzle (0.4×0.02 cm) and was vertically uniform through the depth of the upper layer because the momentum flux into the lower layer was negligible ($\nu \gg \nu_*$).

2. Starting jet: the force acts continuously

Some years ago we studied experimentally a jet developing in homogeneous and non-homogeneous fluids (Voropayev & Filippov 1985). The experiments in a non-homogeneous fluid were done in a linearly stratified fluid (buoyancy frequency $N \approx$ const). When a source of momentum is turned on, a spherical vortex appears. Initially the vortex develops as in a homogeneous fluid because the inertia force exceeds the gravity force. With increasing distance, the gravity force begins to prevail and the initially spherical vortex becomes flat and expands horizontally, forming a frontal vortex dipole (see figure 2). After that the shape of the vortex front does not change and the flow develops self-similarly up to a large distance x from the origin (in our experiments $x/D \approx 1500$) and the lengthscale of the flow increases with time as $t^{\frac{1}{3}}$ (Voropayev & Filippov 1985).

The results of the experiments in a homogeneous fluid were explained theoretically by Voropayev (1985). Below we shall consider a physical model which explains our experimental results in a stratified fluid. This model is based on a scheme shown in figure 4. Suppose that the starting jet consists of two regions: the steady jet region and the front region moving forward with a velocity $\bar{U}$. For our model we need velocity distributions in a jet region, so we consider the steady jet first.

2.1. *Steady jet in a stratified fluid*

When the front region is far away from the origin, the jet behind the front can be considered steady. First, using the technique proposed by Stern & Voropayev (1984), we measured the longitudinal velocity $U_0(x)$ along the axis of the jet behind the front. A weak disturbance was introduced into the jet. As shown by Stern & Voropayev (1984), a weak disturbance propagates with exactly the local velocity of the fluid at the axis of the jet. We took motion pictures of the travelling disturbance from a shadowgraph screen and plotted the position of the disturbance with time. In these flows the origin is a virtual one and is at some distance x_0 behind the nozzle. In an ideal jet from a point source of momentum, the mass flux $Q(x)$ is equal to Q_* at some distance x_0 from the point source. Using Schlichting's formula $Q = 8\pi\rho\nu x$ we have the estimate $x_0 = Q_*/8\pi\rho\nu$. Small values of x_0 were used to correct experimental data. These corrected data for two experiments are shown in figure 5. In every experiment the distance $(x+x_0)$ of the disturbance from the virtual origin increases with time as $(x+x_0) \sim t^{\frac{1}{3}}$. Thus, for $x \gg x_0$, with good accuracy we can take $x \sim t^{\frac{1}{3}}$. Summing up the results of our measurements over the range of governing parameters $J_*/\rho = 10^{-2}$–1.0 cm^4 s^{-2}, $N = 0.4$–2.0 s^{-1}, $x = 1$–40 cm, we have obtained the relation $x = (2A\nu Jt)^{\frac{1}{3}}$, where the non-dimensional force $J = J_*/\rho\nu^2$ and $A = $ const. (figure 6). This dependence is equivalent to

$$U_0(x) = A\nu J/x, \tag{2.1}$$

where U_0 is the longitudinal velocity along the axis of the jet. We have obtained the value $A = 0.12 \pm 0.02$, which is practically equal to Schlichting's value ($A = \frac{3}{8}\pi$) for a steady axisymmetric jet in a homogeneous fluid (Schlichting 1955). Longitudinal velocity distributions across the jet were measured at different distances ($x = 5$–20 cm) from the nozzle. Typical distributions obtained are shown in figure 7 (points

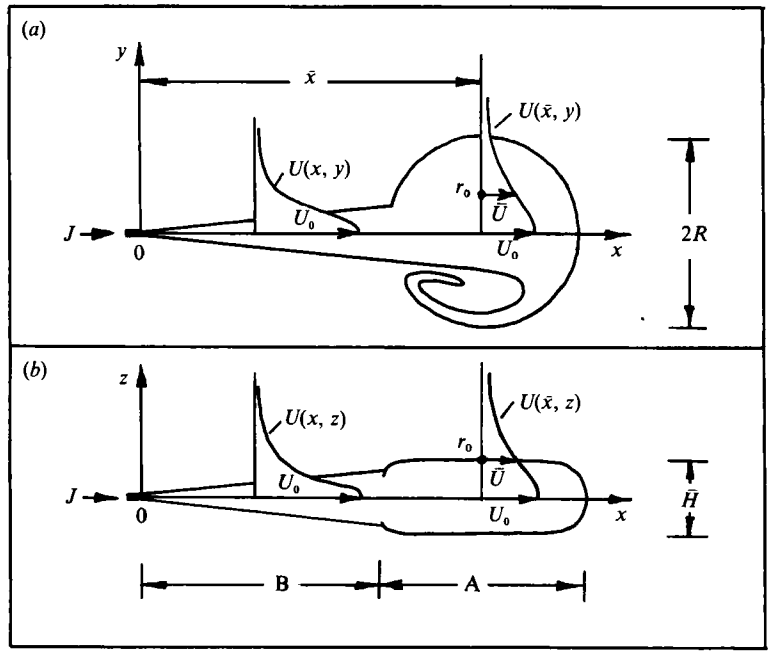

FIGURE 4. Sketch of a starting jet in a stratified fluid: (*a*) top view, (*b*) side view. A, front region, B, jet.

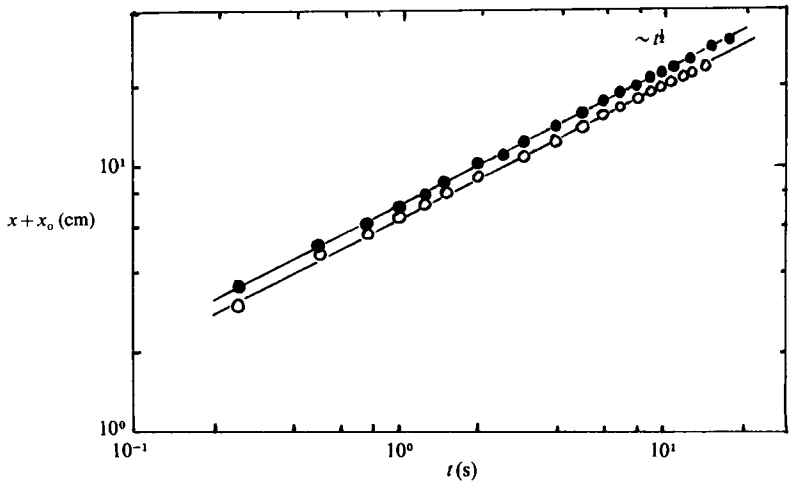

FIGURE 5. Distance $(x+x_0)$ of the 'weak' disturbance along the jet axis from the virtual origin versus time (t): ●, $N = 0.55\ \mathrm{s}^{-1}$, $J = 1.1 \times 10^4$, $x_0 = 0.2$ cm; ○, $N = 0.48\ \mathrm{s}^{-1}$, $J = 1.4 \times 10^4$, $x_0 = 0.5$ cm.

are due to the digitizing of the marker profiles). Self-similar coordinates $Ux/A\nu J$, $B^{\frac{1}{2}}J^{\frac{1}{2}}y/x, B^{\frac{1}{2}}J^{\frac{1}{2}}z/x$ ($A = \frac{3}{8}\pi, B = \frac{3}{64}\pi$) are used to compare the velocity distributions in a stratified fluid with the velocity distribution in an axisymmetric jet in a homogeneous fluid. This theoretical Schlichting's distribution has the form (Schlichting 1955)

$$U = \frac{A\nu J}{x(1+BJr^2/x^2)^2}, \tag{2.2}$$

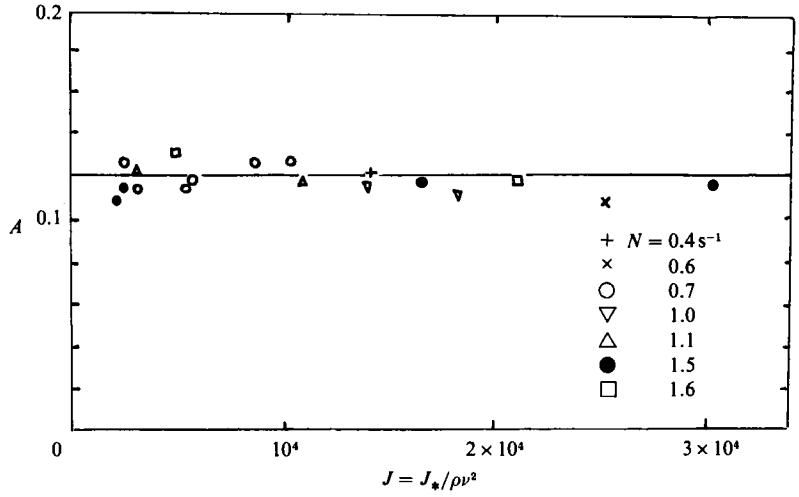

FIGURE 6. Mean values of A versus non-dimensional force $J = J_*/\rho\nu^2$ for experiments with various N.

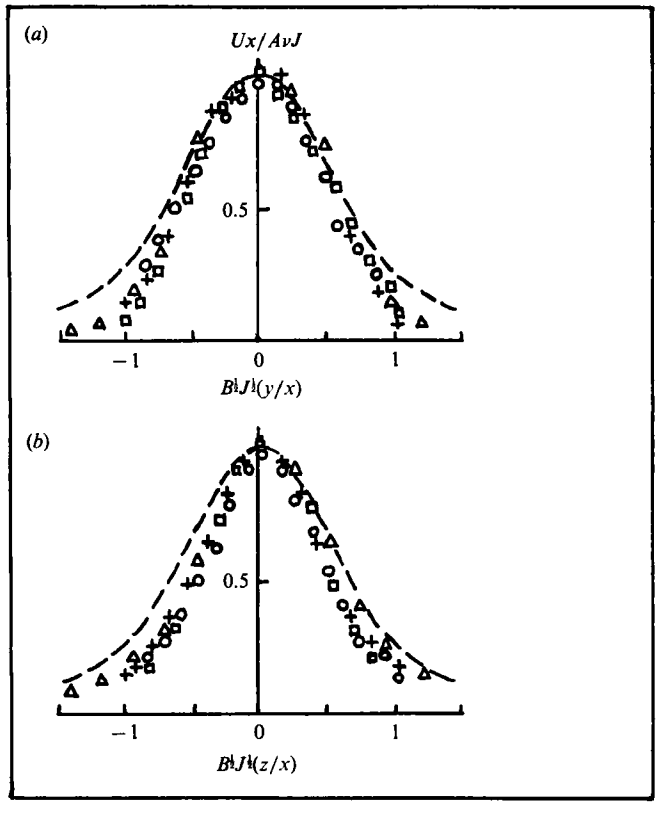

FIGURE 7. Distributions of the longitudinal velocity in a jet in a stratified fluid: (*a*) in the horizontal plane ($z = 0$), (*b*) in the vertical plane ($y = 0$). Symbols: experiments with $N = 0.7\ s^{-1}$ and △, $Re = 99$, $Ri = 0.24$, $x = 5$ cm; □, 69, 0.25, 10 cm; +, 96, 2.27, 15 cm; ○, 50, 14.34, 20 cm. ----, Schlichting's distribution (2.2) in a homogeneous fluid.

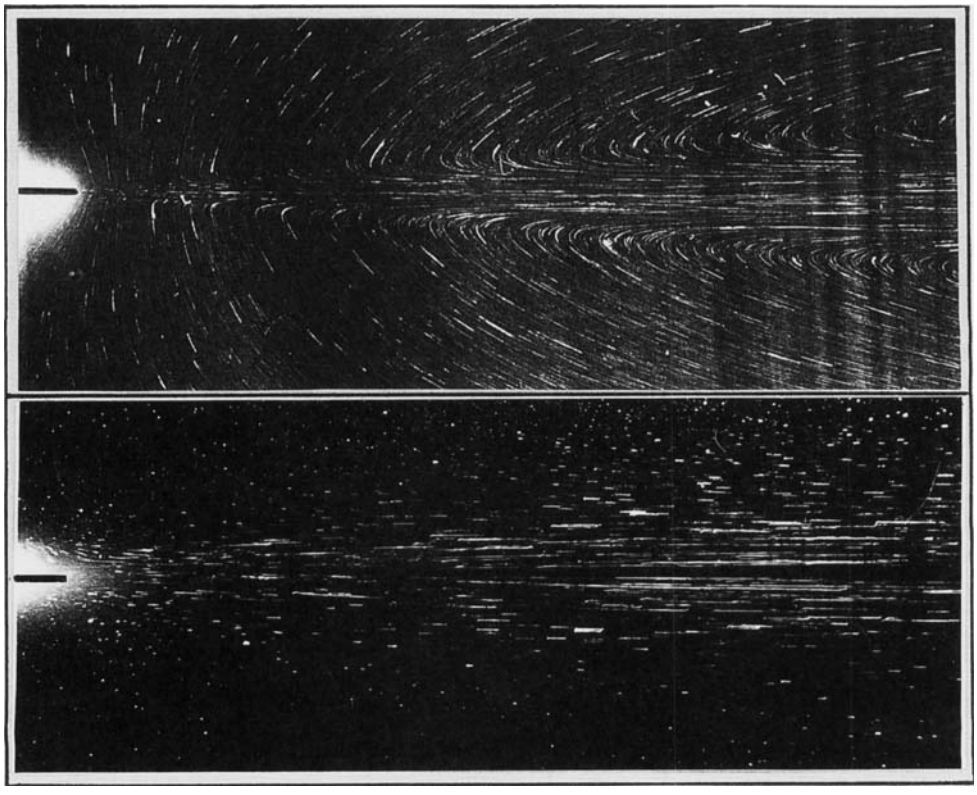

FIGURE 8. Streakline photographs of a jet in a stratified fluid at $N = 0.7\ \mathrm{s}^{-1}$, $Re = 145$, visualized with aluminium powder, exposure 6 s. (*a*) Top view ($z = 0$), (*b*) side view ($y = 0$). The black horizontal line at the left is the nozzle.

$r = (y^2 + z^2)^{\frac{1}{2}}$ being the distance from the jet axis. In figure 7 one can see that the velocity distributions in a stratified fluid are self-similar, vertical and horizontal distributions differ very little and (2.2) is a good approximation for both of them. We should note that these results are not obvious. On the streak pictures (figure 8) one can see that the flow is different in the horizontal and vertical planes. (The slow flow towards the source at large distances from the jet axis in figure 8 is a compensative flux due to the finite dimensions of the experimental tank; note that the velocity measurements presented in figure 7 were made in a narrow cone near the axis of the jet where the influence of the backward compensative flow is negligible.) The vertical velocity is practically absent (except for the immediate vicinity of the orifice) but the horizontal velocity (lateral) is present. From these pictures only one may expect that the velocity distributions in the horizontal ($z = 0$) and vertical ($y = 0$) planes will be different, but the measurements demonstrate that this is not so (figure 7).

We can introduce the Reynolds and the Richardson numbers of the jet, choosing the velocity on the jet axis $U_0 = A\nu J/x$ as the velocity scale of the flow, and the cross-width of the jet $H = x/B^{\frac{1}{2}}J^{\frac{1}{2}}$ as the lengthscale of the flow,

$$Re = HU_0/\nu = AJ^{\frac{1}{2}}/B^{\frac{1}{2}} \approx J^{\frac{1}{2}}, \tag{2.3}$$

$$Ri = H^2N^2/U_0^2 = N^2x^4/\nu^2A^2BJ^3. \tag{2.4}$$

As one may expect, the Reynolds number is constant along the jet but the Richardson number increases rapidly with the distance x from the origin. Data

shown in figure 7 were obtained in experiments where Ri varied by a factor of 60 but one can see that velocity distributions are approximately the same. (A theoretical explanation of this result on the basis of the Navier–Stokes equations for the asymptotic case $Re \gg 1$, $ReRi \geqslant 1$ is given in Voropayev 1989.) For further analysis we shall use (2.2) as an approximation of the longitudinal velocity distribution in a steady jet in a stratified fluid.

2.2. *Front region of a starting jet: empirical model*

The front region as a whole moves with a velocity which is less than the local velocity of the fluid in a jet behind the front. So the fluid from the jet always flows into the front region. This fluid then spreads horizontally, forming a vortex dipole. We shall consider the details of the fluid motion in this dipole below in §2.3. Here, it is essential to know only that its shape is similar at any instant of time. Observations demonstrate (see figures 2, 9) that the front region looks like a flat disk with a streamlined shape and moves with a velocity

$$\bar{U} = \mathrm{d}\bar{x}/\mathrm{d}t, \tag{2.5}$$

where $\bar{x}$ is the distance of the front-region centre from the origin. The results of measurements (Voropayev & Filippov 1985) show that the horizontal cross-width of the front region ($2R$) and the distance $\bar{x}$ increase with time accurately as $t^{\frac{1}{2}}$. Hence we can say that the lengthscale of the flow varies in a similar manner, and using (2.1) we have

$$2R = \alpha\bar{x}, \tag{2.6}$$

$$\bar{U} = \beta U_0, \tag{2.7}$$

$$\bar{H} = 2\gamma\bar{x}, \tag{2.8}$$

where $\bar{H}$ is the mean vertical thickness of the front region, and α, β, γ are non-dimensional coefficients which do not depend on $\bar{x}$. We want to calculate the values of these coefficients. The agreement between the theoretical and experimental values of α, β, γ will be a criterion for our model correctness.

Following papers by Abramovich & Solan (1973) and Voropayev (1985), we shall use an integral model to describe the front-region motion (figure 4). Let us consider the front region as a liquid volume $\bar{V}$ moving forward with the velocity $\bar{U}$. The jet which flows into the rear of the front region has a velocity distribution (2.2) and transports some momentum and mass into the front region. The equations of conservation of mass and momentum for liquid volume $\bar{V}$ are

$$\frac{\mathrm{d}\bar{V}}{\mathrm{d}t} = 2\pi\int_0^{r_0}(U-\bar{U})\,r\,\mathrm{d}r + \frac{\bar{Q}}{\rho}, \tag{2.9}$$

$$(1+k)\frac{\mathrm{d}(\bar{U}\bar{V})}{\mathrm{d}t} = 2\pi\int_0^{r_0}U(U-\bar{U})\,r\,\mathrm{d}r - \frac{\bar{F}}{\rho} \tag{2.10}$$

($k = 0.5$ is the virtual-mass coefficient).

The drag force $\bar{F}$ and the additional mass influx $\bar{Q}$ will be defined below. The condition which determines the distance (r_0) from the jet axis where the velocity in a jet (U) is equal to the front-region velocity ($\bar{U}$) is

$$U(r_0, \bar{x}) = \bar{U}(\bar{x}). \tag{2.11}$$

Using (2.2), (2.5), (2.7), (2.11), we have

$$r_0 = (1-\beta^{\frac{1}{2}})^{\frac{1}{2}}\bar{x}/B^{\frac{1}{2}}\beta^{\frac{1}{4}}J^{\frac{1}{2}}. \tag{2.12}$$

(a)

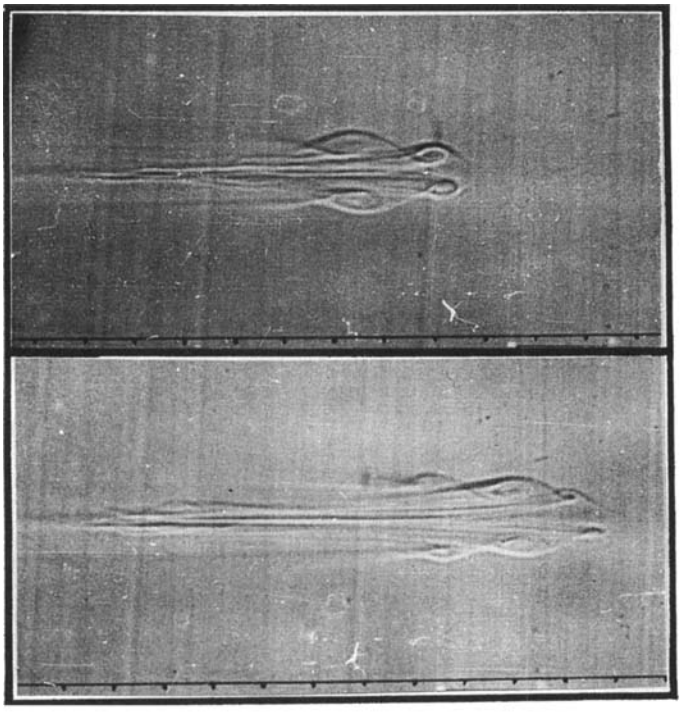

(b)

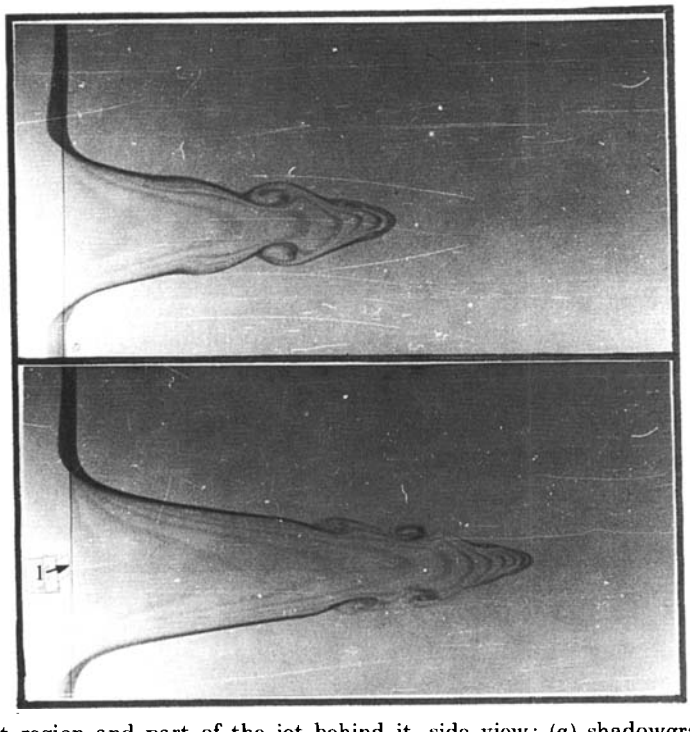

FIGURE 9. Front region and part of the jet behind it, side view: (a) shadowgraph picture, (b) thymol-blue visualization; 1, platinum wire ($x = 17$ cm, $y = 0$), $N = 1.5$ s^{-1}, $Re = 104$; scale in cm.

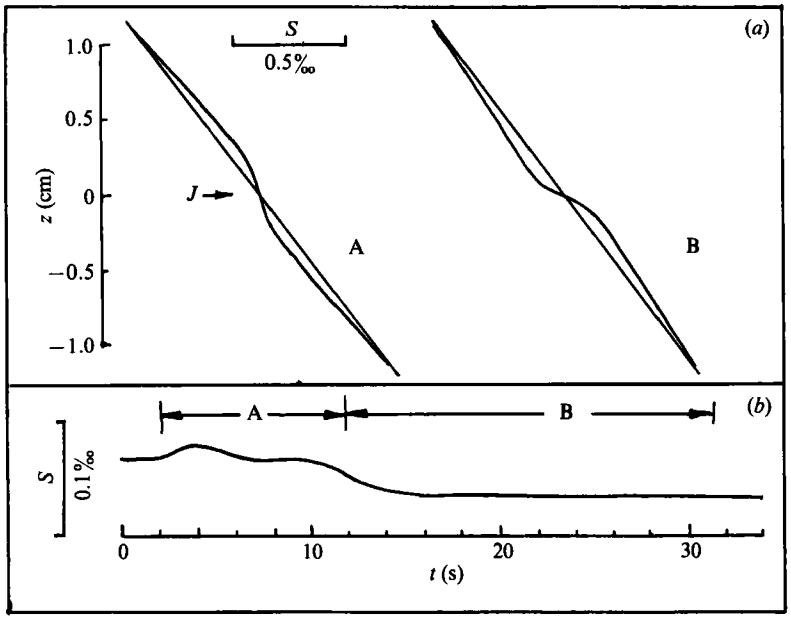

FIGURE 10. (*a*) Vertical profiles of salinity in the starting jet and (*b*) time variation of salinity at a point. A, front region; B, jet; (*a*) $x = 5$ cm, $y = 0$; (*b*) $x = 5$ cm, $y = 0$, $z = 1$ cm. $Re = 170$. The straight lines in (*a*) show the undisturbed profile.

Fluid particles with $r > r_0$ move slower than the front region and never enter it. Thus an estimate for the mean value of the front-region thickness is

$$\bar{H} = 2r_0. \tag{2.13}$$

Hence the coefficient γ in (2.8) is determined and we shall look for α and β. Using (2.13) we can write the following estimate for the liquid volume:

$$\bar{V} = 2\pi R^2 r_0. \tag{2.14}$$

Consider now a flat liquid disk with radius R and height $\bar{H}$, intruding horizontally into the linearly stratified resting fluid. In general the drag force $\bar{F}$ in (2.10) is the sum of the wave (F_w) and the viscous (F_ν) drag forces.

Typical 'instantaneous' salinity profiles across the front and jet regions of the flow are shown in figure 10(*a*). One can see that the fluid particles in the front region are displaced from the plane $z = 0$. By contrast, the fluid particles in the jet region are sucked towards the plane $z = 0$. The displacement is small and decreases rapidly with distance from the origin. Thus the density distribution in the flow when x is not small are practically the same as in the ambient fluid. The time record shown in figure 10(*b*) demonstrates that there are no significant internal waves in the flow. Small changes in the salinity on this record are due to the small displacement of fluid particles in the jet and front regions from their equilibrium levels. Hence the amplitudes of the internal waves are very small and the wave drag (F_w) is negligible.

The viscous drag on a disk is determined mainly by the friction on its horizontal surfaces and we can use the estimate

$$\bar{F} \approx F_\nu = c\nu\rho R\bar{U}, \tag{2.15}$$

where $c = \frac{32}{3}$ (Lamb 1932). The leading edge of the starting jet, intruding into the

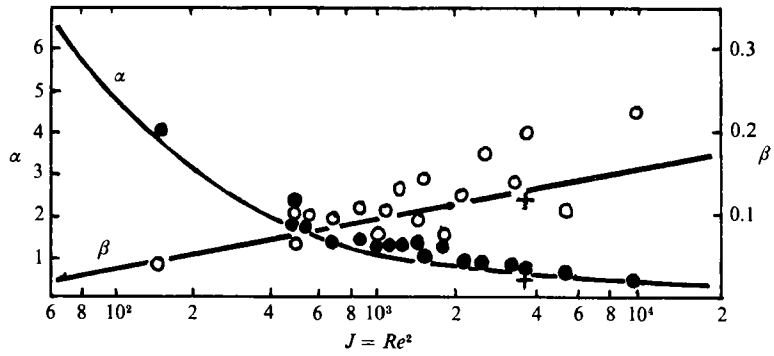

FIGURE 11. Measured (symbols, $N = 0.5$–$2.5\ \mathrm{s}^{-1}$) and calculated (from (2.17), (2.18), solid lines, $\lambda = 0.3$) α (●) and β (○) for different $J = Re^2$. Crosses show the results of a three-dimensional numerical simulation by Voropayev & Neelov (1991).

resting fluid, splits up into two symmetric 'half-jets' which then wrap into spirals, forming the disk-like shape of the front region. On the outer boundary of these half-jets the initially quiescent ambient fluid forms a viscous boundary layer. Some fluid from this boundary layer entrains into the front region, giving the additional influx $\bar{Q}$ in the mass conservation equation (2.9). The total flux Q in a steady round jet increases linearly with the distance x from the origin: $Q = 8\pi\nu\rho x$ (Schlichting 1955). One can interpret the steady jet as a free boundary layer and estimate the term $\bar{Q}$ using this formula. In our case the distance x must be measured from the splitting point and it is equal to the arclength of the disk-like front region: $x \approx \pi R$. For two 'half-jets' we have the estimate

$$\bar{Q} \approx \lambda 8\pi^2 \nu\rho R. \tag{2.16}$$

In a self-similar flow λ must be a constant. Its value is equal to the portion of fluid which enters from the boundary layer (on the outer boundary of the front region) into the front region ($\lambda < 1$). In our model the value of λ is not known but must be found from a comparison of calculated and measured values for α and β.

Thus the system of governing equations is closed. Not taking into account the exact initial conditions (nozzle size, flux rate Q_* at the nozzle exit) one can look for solutions in the self-similar form (2.6), (2.7). Recall that we have already determined the coefficient γ in (2.8). Integrating (2.9), (2.10), and using (2.1), (2.2), (2.5), (2.11), (2.12), (2.14)–(2.16) for solutions in the form (2.6), (2.7) we have two algebraic equations for α and β:

$$(3^{\frac{5}{2}}/8\pi^{\frac{1}{2}})\,\alpha^2\beta^{\frac{3}{4}}(1-\beta^{\frac{1}{2}})J^{\frac{1}{2}} = 2(1-\beta^{\frac{1}{2}})^2 + \lambda\alpha\pi, \tag{2.17}$$

$$(2\times 3^{\frac{3}{2}}/\pi^{\frac{1}{2}})\,(1+k)\,\alpha^2\beta^{\frac{7}{4}}(1-\beta^{\frac{1}{2}})^{\frac{1}{2}}J^{\frac{1}{2}} = (2^4/3)\,(1-3\beta+2\beta^{\frac{3}{2}}) - c\alpha\beta. \tag{2.18}$$

The results calculated from (2.17), (2.18) and experimental values of α and β are shown in figure 11. The experimental values of α and β were determined by using the data from our previous experiments (Voropayev & Filippov 1985). In that paper we obtained the relation $\bar{x} \sim t^{0.45}$ for the starting jet in a stratified fluid ($N \neq 0$). This small but systematic difference of the power from $\frac{1}{2}$ puzzled us but we were unable to explain it. The difference is important, and now we shall show how it arises. The self-similar regime for a jet in a stratified fluid originates not from the origin but at some small distance (x_*) from it where $\overline{Ri}\,(x_*) \approx 1$ ($\overline{Ri} = \bar{H}^2\bar{N}^2/\bar{U}^2 \sim x^4/J^3$ is the

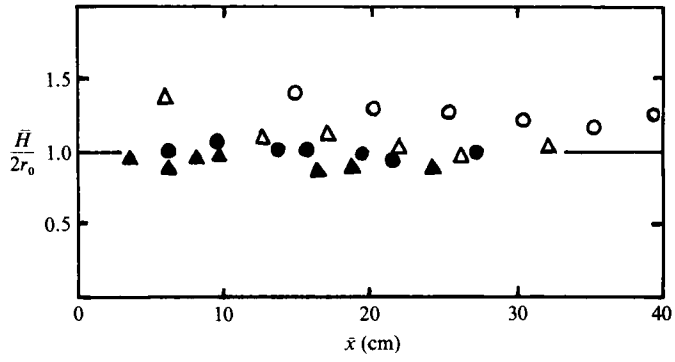

FIGURE 12. Non-dimensional thickness ($\bar{H}/2r_0$) of the front region for different distances ($\bar{x}$) from the origin. $N = 1.4\ \mathrm{s}^{-1}$; ▲, $Re = 56$; ●, 73; △, 107; ○, 146.

Richardson number of the front region). When $\bar{x} < x_*$ the stratification does not play any significant role, the flow develops as in a homogeneous fluid and the front region has a spherical form. At $\bar{x} > x_*$ the front region flattens and transforms to a disk. Its rear entrance widens horizontally and an additional influx $\bar{Q}$ becomes important. The dynamics of the flow changes so that α increases and β decreases compared with the homogeneous fluid (see Voropayev 1985). When all experimental points were corrected using small values of x_* they lay exactly on the curves $\bar{x} \sim t^{\frac{1}{2}}$. Using data corrected in this way, experimental values of α and β were determined.

In (2.17), (2.18) λ is a free parameter. Its value ($\lambda = 0.3$) was chosen by fitting of the experimental and calculated values of α and β. It turns out that the exact value of the drag force coefficient c (and the virtual-mass coefficient k) does not enter very sensitively in the calculations; thus the drag force influence on the flow dynamics is negligible. The momentum flux transported by the jet into the front region goes mainly to the acceleration of the initially quiescent fluid entrained into the front region. The calculated and experimental values of α and β as functions of $J = Re^2$ are shown in figure 11. Knowing β we can verify the relation (2.13). In our previous experiments (Voropayev & Filippov 1985) the thickness $\bar{H}$ of the front region was not measured. Using the simple technique proposed by Gärtner (1983) we have made these measurements and the results are shown in figure 12 in a non-dimensional form (the values of r_0 for different $\bar{x}$ and J were calculated using the relation (2.12) and the graph in figure 11).

Introducing the Reynolds number of the front region

$$\overline{Re} = 2R\bar{U}/\nu = \alpha\beta AJ \tag{2.19}$$

and using (2.1), (2.5)–(2.7), (2.13), we can write some useful estimates:

$$\bar{x} = (2\overline{Re}/\alpha)^{\frac{1}{2}}(\nu t)^{\frac{1}{2}}, \tag{2.20}$$

$$R = (\tfrac{1}{2}\alpha\overline{Re})^{\frac{1}{2}}(\nu t)^{\frac{1}{2}}, \tag{2.21}$$

$$\bar{U} = (\overline{Re}/2\alpha)^{\frac{1}{2}}(\nu/t)^{\frac{1}{2}}, \tag{2.22}$$

$$\bar{H} = 8\beta^{\frac{1}{4}}(1-\beta^{\frac{1}{2}})(\nu t)^{\frac{1}{2}}. \tag{2.23}$$

From (2.20), (2.22) we have a simple estimate for the 'age' of the flow:

$$t = \bar{x}/2\bar{U}. \tag{2.24}$$

Thus our model gives all integral characteristics of the starting jet if the main governing parameter $J = Re^2$ is known. Below, on the basis of the analytical solution, we shall consider a model of vortex dipole generation in a viscous fluid and study the internal structure of the unsteady dipole.

2.3. *A model of vortex dipole generation: experimental verification of the analytical solution*

For simplicity consider the plane flow of a viscous incompressible fluid induced by a momentum source which starts at time $t = 0$ and thereafter exerts a force I_*/ρ (units of length^3/time^2) per unit mass on the fluid in a direction $\theta = 0$ in polar coordinates (r, θ). The source is at the point $r = 0$. The governing equations are

$$\omega_t + u\omega_r + \frac{1}{r} v\omega_\theta = \nu\left(\frac{1}{r^2}\omega_{\theta\theta} + \frac{1}{r}(r\omega_r)_r\right), \tag{2.25}$$

$$r\omega = (rv)_r - u_\theta, \tag{2.26}$$

$$u = \frac{1}{r}\psi_\theta, \quad v = -\psi_r \tag{2.27}$$

$$\left(\omega_t \equiv \frac{\partial\omega}{\partial t}, \ldots, \quad \psi_r \equiv \frac{\partial\psi}{\partial r}\right),$$

where ω is the vorticity and ψ the stream function. Initially the fluid is at rest. The motion at infinity is absent. The integral balance of forces acting in the direction $\theta = 0$ on a fluid contained in a circle of radius R with its centre at the origin $(r = 0)$ must be added to the governing equations;

$$\frac{I_*}{\rho} = \int_0^{2\pi}\int_0^R \frac{\partial}{\partial t}(u\cos\theta - v\sin\theta)\, r\, \mathrm{d}r\, \mathrm{d}\theta + R\int_0^{2\pi}\left[u(u\cos\theta - v\sin\theta) - \left(\frac{\sigma^{rr}}{\rho}\cos\theta - \frac{\sigma^{r\theta}}{\rho}\sin\theta\right)\right]\mathrm{d}\theta \tag{2.28}$$

(σ^{rr}, $\sigma^{r\theta}$ are the stresses). Stokes' solution for (2.25)–(2.28) is (Cantwell 1986; Afanasyev & Voropayev 1989)†:

$$\psi = \frac{I_* r}{2\pi\rho\nu}\left[\frac{\nu t}{r^2}(1 - \mathrm{e}^{-r^2/4\nu t}) + \tfrac{1}{4}E_1(r^2/4\nu t)\right]\sin\theta, \tag{2.29}$$

$$\omega = \frac{I_*}{2\pi\rho\nu r}\mathrm{e}^{-r^2/4\nu t}\sin\theta, \tag{2.30}$$

where

$$E_1(z) = \int_1^\infty \mathrm{e}^{-zt}\, t^{-1}\, \mathrm{d}t$$

is an integral exponent.

Though this asymptotic solution is obtained for a linear approximation, it is very helpful for a better understanding of the real flow evolution.

In experiments some passive tracer is used to visualize the flow: it is usually a dye.

† Our numerical values of coefficients in (2.29), (2.30) are two times greater than those given by Cantwell (1986). It seems that there is an arithmetic error in the formula (5.1) in his paper.

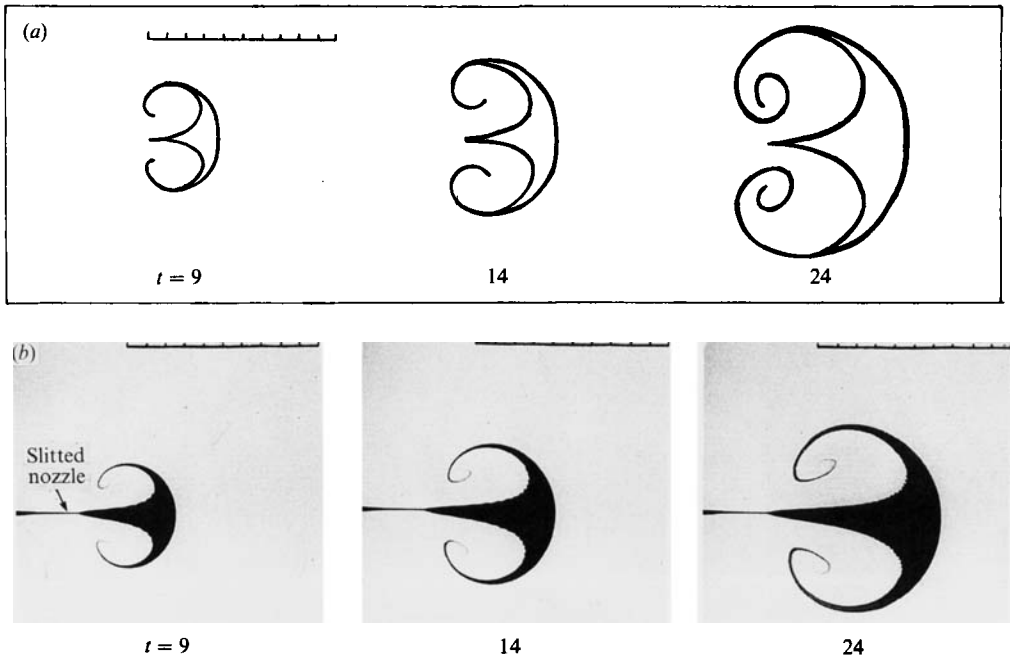

FIGURE 13. Plane starting jet, the source of momentum acts continuously: (*a*) calculations with the stream function (2.29) for $\nu = 2.7 \times 10^{-2}$ cm^2 s^{-1}, $I/\rho = 2.8$ cm^3 s^{-2}; (*b*) experiment in a layer of viscous ($\nu = 2.7 \times 10^{-2}$ cm^2 s^{-1}) fluid lying on a heavier fluid with low ($\nu_* = 5 \times 10^{-3}$ cm^2 s^{-1}) viscosity, $I/\rho = 2.8$ cm^3 s^{-2}. Scales in cm, time (t) in s.

Equations of motion for marked particles with the stream function (2.29) have the form

$$\frac{\mathrm{d}r}{\mathrm{d}t} = \frac{I_*}{2\pi\rho\nu}\left[\frac{\nu t}{r^2}(1-\mathrm{e}^{-r^2/4\nu t}) + \tfrac{1}{4}E_1\left(\frac{r^2}{4\nu t}\right)\right]\cos\theta, \tag{2.31}$$

$$\frac{\mathrm{d}\theta}{\mathrm{d}t} = \frac{I_*}{2\pi\rho\nu r}\left[\frac{\nu t}{r^2}(1-\mathrm{e}^{-r^2/4\nu t}) - \tfrac{1}{4}E_1\left(\frac{r^2}{4\nu t}\right)\right]\sin\theta. \tag{2.32}$$

Integrating these equations numerically one can calculate the trajectory of a marked particle starting at $t = t_0$ from the point (r_0, θ_0).

In our experiment a dyed fluid is injected continuously from a thin slitted nozzle (of width $d = 0.02$ cm). In computations the marked particles were injected discretely from several points on the arc $r_0 = \frac{1}{2}d$, $-\frac{1}{2}\pi \leqslant \theta_0 \leqslant \frac{1}{2}\pi$ at small time intervals. The end points of all injected particles at time t give the theoretical distributions of 'dyed' fluid shown in figure 13(*a*). For comparison photos of the real flow in a thin layer of viscous fluid are shown in figure 13(*b*). In spite of essential simplifications, the model correctly reproduces the general features of the flow – its spiral structure – and is in quite good agreement with the observations. Certainly, the three-dimensional numerical simulation in a stratified fluid (Voropayev & Neelov 1991) gives more realistic information about the real flows, but that is not a primary task of our paper.

3. Impulsive vortex dipole

In these experiments a strong horizontal jet was injected for a short period of time (Δt) into a density-stratified fluid at the level of its equilibrium density. The jet transports the horizontal momentum $P_* = 4Q_*^2\,\Delta t/\pi D^2\rho$ into the fluid. In a density-

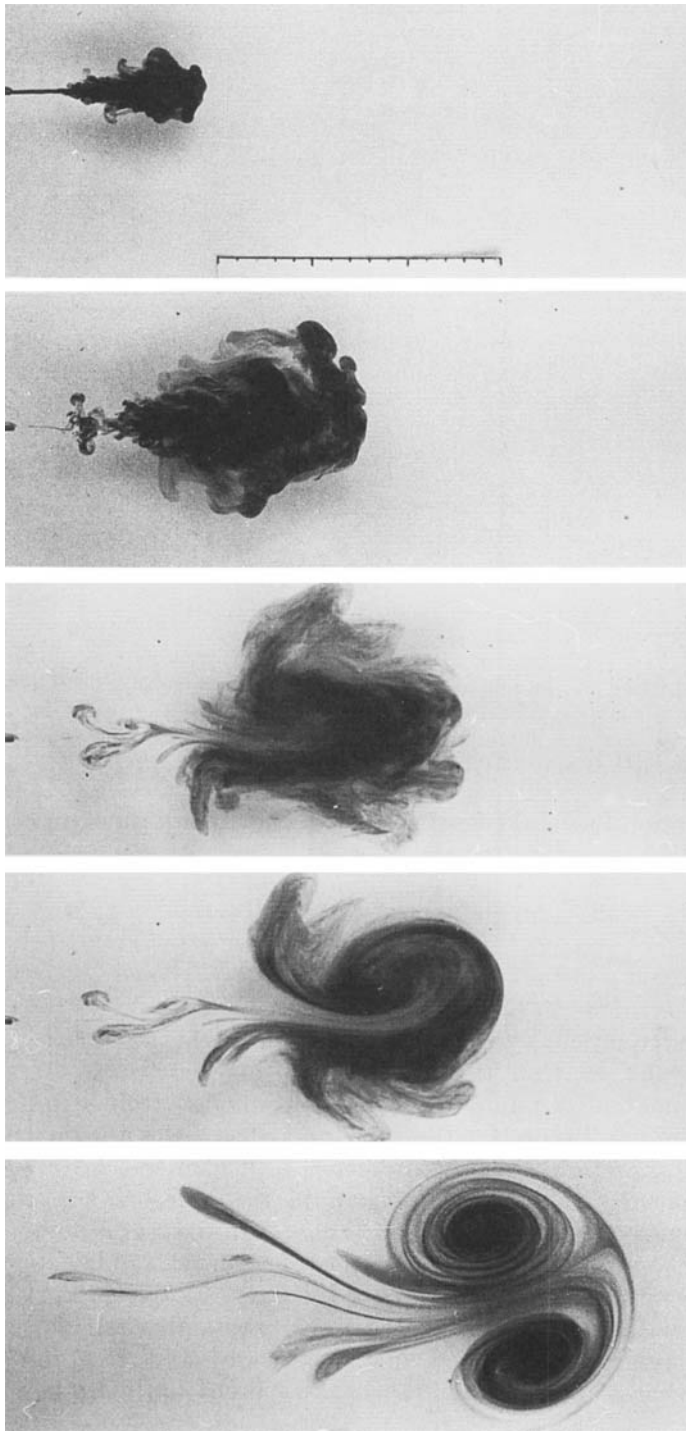

FIGURE 14. Formation of the vortex dipole in a stratified fluid, top view: $N = 1.5\ \mathrm{s}^{-1}$, $\Delta t = 5$ s, $Re = 4Q_*/\pi\nu\rho D = 720$; scale in cm, time ($t$) in s (Voropayev 1987).

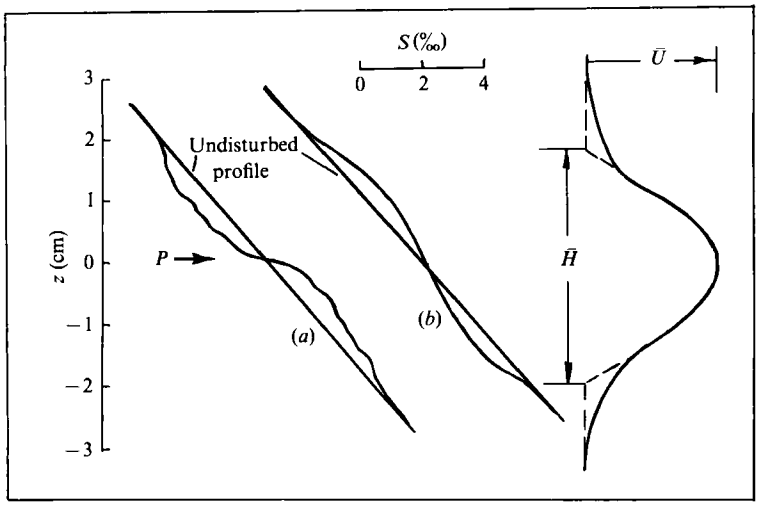

FIGURE 15. Vertical profiles of horizontal velocity (approximately) and salinity in the vortex dipole: (*a*) in a jet-like flow before the vortex dipole is formed ($t < t_0$), (*b*) in the centre of the vortex dipole after it is formed ($t > t_0$), $\Delta t = 4$ s, $Re = 530$.

stratified fluid the vertical motion is suppressed by gravity, and thus the flow rapidly becomes horizontal. The front region of the flow moves with a velocity $\bar{U}$ which is less than the local velocity U_0 of the fluid in the flow behind the front. The vorticity generated by the source of momentum is transported by the jet-like flow into the front region and is concentrated here, forming two flat vortices of opposite sign – a vortex dipole (see figure 14). The formation process finishes in a time of approximately $t_0 \approx \Delta t/(1-\beta)$, when the main part of the moving fluid enters the front region. Here,

$$\beta(Re) = \bar{U}/U_0, \quad 0 < \beta < 1, \quad Re = 4Q_*/\pi D\nu\rho$$

is the initial Reynolds number of the jet-like flow.

The vortex dipole formed moves forward and its horizontal dimension increases through the entrainment of ambient fluid. Vertical profiles of salinity in the flow before and after the vortex dipole is formed are shown in figure 15. Note that the density distributions in the flow before and after the vortex dipole is formed are similar to the density distributions in the steady jet region and in the front region of the starting jet respectively (see figure 10). Note also that the fluid in a vortex dipole is hardly mixed in a vertical direction.

The observations demonstrate that after the vortex dipole is formed its shape is similar at any instant of time. For simplicity we shall consider a vortex dipole as a liquid disk of thickness $\bar{H}$, diameter $2R$, moving with a velocity $\bar{U} = \mathrm{d}\bar{x}/\mathrm{d}t$ ($\bar{x}$ is the distance of the centre of the disk from the origin).

3.1. *Vortex dipole characteristics: scaling analysis*

Using a standard hypothesis (Turner 1964*b*, 1986; Escudier & Maxworthy 1973) the equation of mass balance for the dipole is

$$\pi \frac{\mathrm{d}\bar{H}R^2}{\mathrm{d}t} = \frac{\bar{Q}}{\rho}, \tag{3.1}$$

where $\bar{Q} = \pi\alpha\rho\bar{H}R\bar{U}$, and α is the entrainment coefficient.

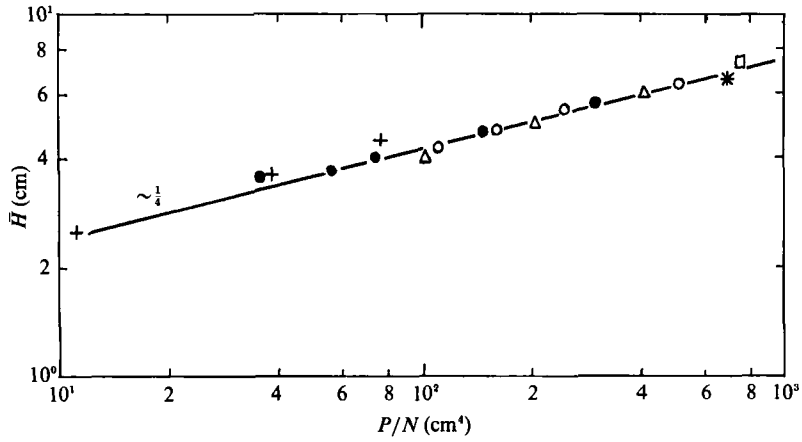

FIGURE 16. Vortex dipole thickness $\bar{H}$ versus P/N: momentum P was varied by variation of Q_*/ρ (0.5–3.0 cm^3 s^{-1}) and Δt (1–8 s). Symbols denote experimental points with different values of P (50–400 cm^4 s^{-1}) and N (0.5–2.5 s^{-1}). Each symbol represents a particular value of Q_*. Solid line is (3.4) with $\gamma = 1.4$.

The momentum conservation equation is

$$(1+k)\,\pi\frac{\mathrm{d}\bar{H}R^2\bar{U}}{\mathrm{d}t} = \frac{-F}{\rho}, \tag{3.2}$$

where $k = 1$ is a virtual-mass coefficient, and $F = c\nu\rho R\bar{U}$, similar to (2.15), is the viscous drag force applied on the horizontal boundaries of the dipole. For solving (3.1), (3.2) data on the dipole thickness $\bar{H}$ are needed. In general, $\bar{H}$ can depend on the kinematic momentum $P = P_*/\rho$, the buoyancy frequency N, time t and viscosity ν. On dimensional grounds

$$\frac{\bar{H}N^{\frac{1}{4}}}{P^{\frac{1}{4}}} = f(\tau_0, \tau_*), \tag{3.3}$$

where $\tau_0 = Nt$, $\tau_* = \nu N^{\frac{1}{2}}t/P^{\frac{1}{2}}$ are dimensionless times. In our experiments we used a strong jet to exert a large momentum for a short period of time on the fluid. Typical values of the governing parameters are: $P \approx 10^2$ cm^4 s^{-1}, $N \approx 1$ s^{-1}, $\Delta t \approx 5$ s, $t \lesssim 10^2$ s. When $t > t_0$ the dipole is formed and $\tau_0 \gg 1$. By contrast, $\tau_* \ll 1$ when t is not too large ($t \lesssim P^{\frac{1}{2}}/\nu N^{\frac{1}{2}}$). Thus, we assume a complete similarity of the function $f(\tau_0, \tau_*)$ with respect to parameters τ_0, τ_*: $f(\tau_0 \gg 1, \tau_* \ll 1) = \text{const.}$ (see, for example, Barenblatt 1979).

The vortex dipole thickness $\bar{H}$ was measured using a simple technique proposed by Gärtner (1983). Observations demonstrate that after the dipole has been formed ($t > t_0$) its thickness $\bar{H}$ does not vary with time, hence $f(\tau_0, \tau_*) = \text{const.} = \gamma$ and

$$\bar{H} = \gamma P^{\frac{1}{4}}/N^{\frac{1}{2}}. \tag{3.4}$$

The results of our measurements (figure 16) for $t_0 \lesssim t \lesssim P^{\frac{1}{2}}/\nu N^{\frac{1}{2}}$ give a mean value $\gamma \approx 1.4$.

Substitution for $\bar{H}$ and for $\bar{Q}$ permits (3.1) to be integrated to give

$$2R = \alpha\bar{x}. \tag{3.5}$$

In the model the coefficient α is not known; its value must be obtained from the

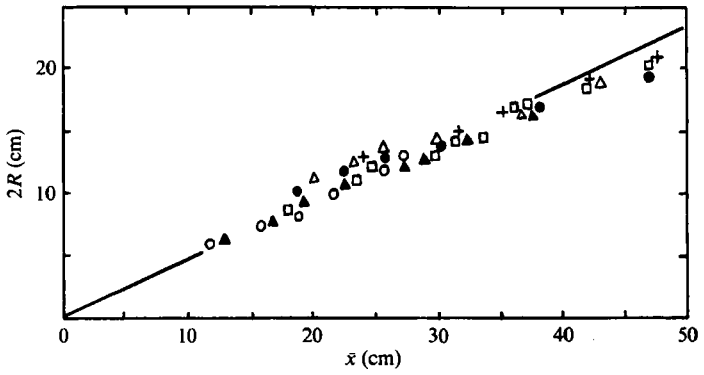

FIGURE 17. Vortex dipole diameter ($2R$) for different distances ($\bar{x}$) from the origin: symbols denote experimental points with different values of P (50–400 cm^4 s^{-1}) and N (0.5–2.5 s^{-1}). Solid line is (3.5) with $\alpha = 0.46$.

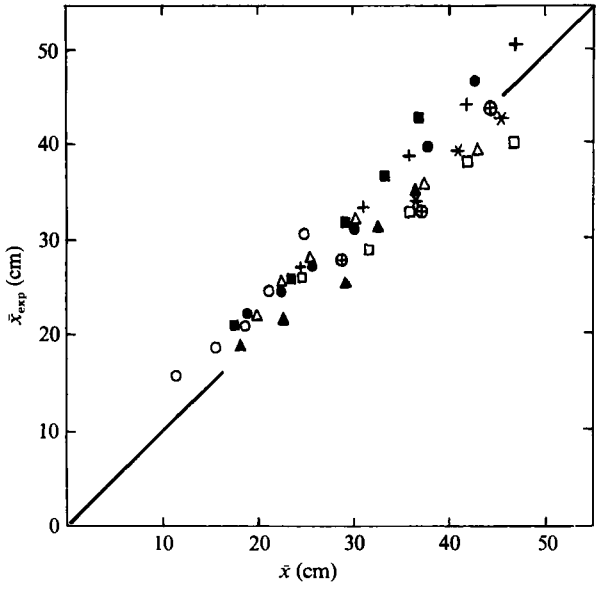

FIGURE 18. Measured $\bar{x}_{\text{exp}}$ and calculated $\bar{x}$ (from (3.7) with $\alpha = 0.46$, $\gamma = 1.4$) distances of the vortex dipole centre from the origin: each symbol denotes different t (10–350 s) but the same P (50–400 cm^4 s^{-1}) and N (0.5–2.5 s^{-1}).

experiment. The results of our measurements (see figure 17) are in good agreement with the estimate (3.5) and give the mean value $\alpha \approx 0.46$.

Substitution for $\bar{H}$, R and F, permits (3.2) to be integrated to give

$$-\bar{x}+\left(\frac{4P}{\alpha c\nu}\right)^{\frac{1}{2}} \operatorname{arctanh}\left[\left(\frac{\alpha c\nu}{4P}\right)^{\frac{1}{2}}\bar{x}\right] = \frac{c\nu N^{\frac{1}{4}}t}{\alpha(k+1)\gamma\pi P^{\frac{1}{4}}}. \tag{3.6}$$

For integration we have used the initial condition that for $t = 0$ ($\bar{x} = 0$), momentum P is applied to the fluid. Expanding (3.6) we obtain the estimate

$$\bar{x} \approx \left[\frac{12}{\alpha^2(1+k)\gamma\pi}\right]^{\frac{1}{3}} N^{\frac{1}{12}} P^{\frac{1}{4}} t^{\frac{1}{3}}. \tag{3.7}$$

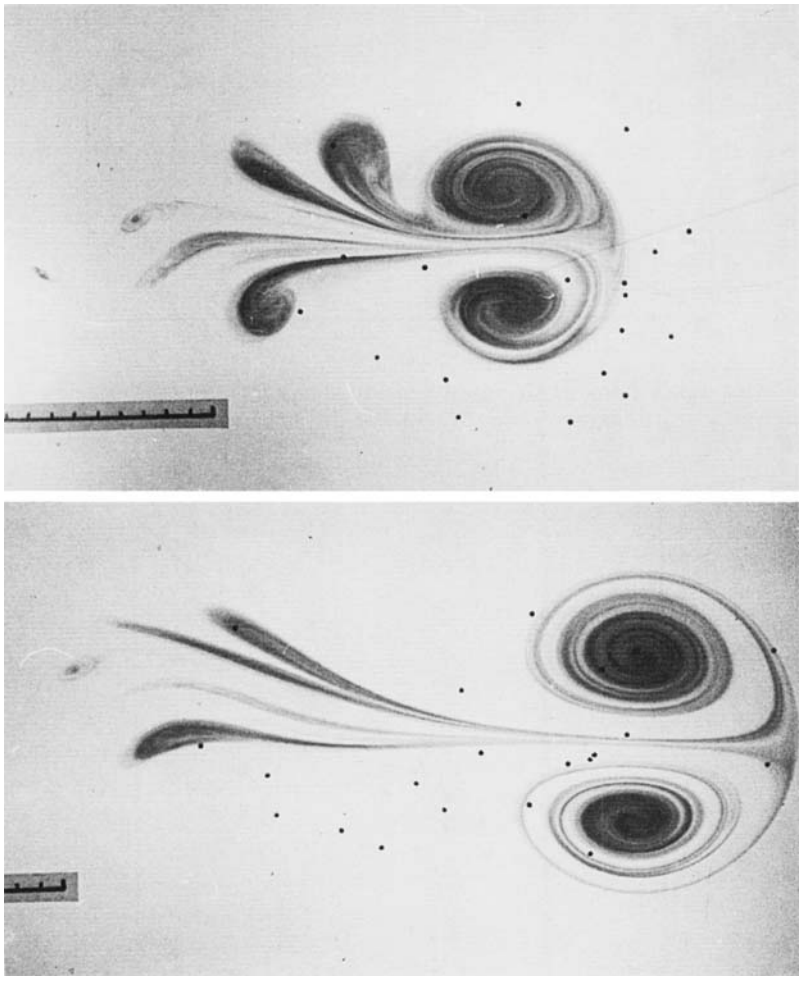

FIGURE 19. The motion of the tracer particles (polystyrol spheres) into the vortex dipole: $P = 125$ cm^4 s^{-1}; (*a*) $t = 32$ s, (*b*) 125 s. Scale in cm.

The calculated results from (3.7) versus experimental values of $\bar{x}$ are shown in figure 18.

Thus, during the intermediate asymptotic regime (intermediate times) the dipole develops self-similarity, its diameter $2R$ and the distance $\bar{x}$ from the origin increase with time as $t^{\frac{1}{3}}$, and the dipole thickness $\bar{H}$ remains constant. Note that the Reynolds number of the flow $\overline{Re} = 2R\bar{U}/\nu \sim t^{-\frac{1}{3}} \sim \bar{x}^{-1}$ decreases with time. By contrast, the Richardson number $\overline{Ri} = \bar{H}^2N^2/\bar{U}^2 \sim t^{\frac{4}{3}} \sim \bar{x}^4$ rapidly increases.

3.2. *Kinematical model of entrainment into an expanding vortex dipole*

In order to understand better the fluid particles' motion into the vortex dipole, we have performed some experiments with the tracer particles. Small polystyrol spheres were introduced into the resting stratified fluid before the start of the experiment. The spheres' density was approximately equal to the fluid density at the nozzle level. In experiments, successive photographs of the flow with the tracer particles were taken (two of these fourteen photographs are reproduced in figure 19). The positions of the spheres were plotted graphically, using the coordinates ($\eta = r/R$, θ) and are

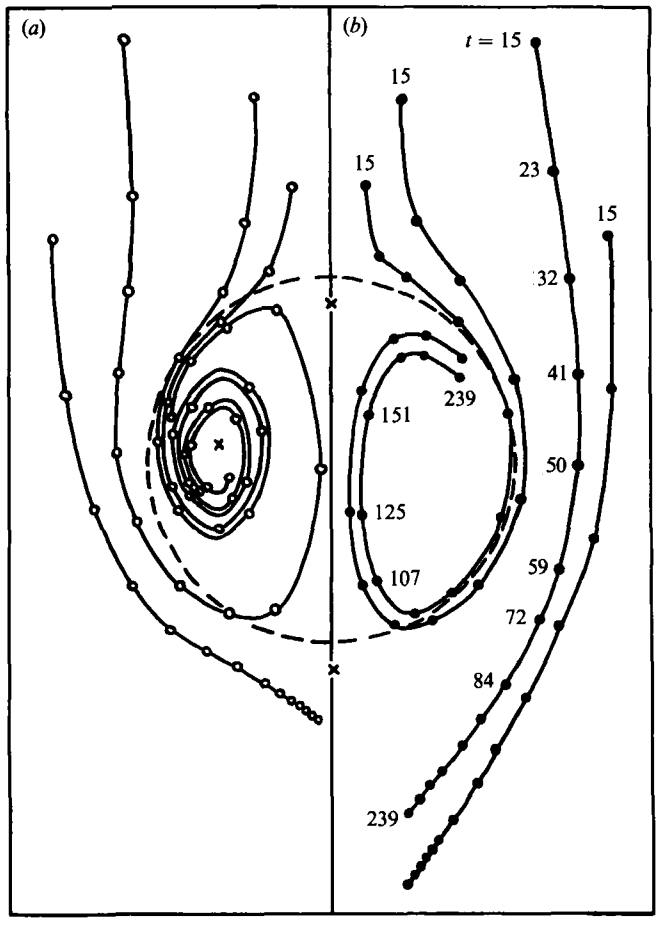

FIGURE 20. Trajectories of four tracer particles in coordinates ($\eta = r/R(t)$, θ): (*a*) calculations, (*b*) experiment; time t in s from the beginning of the experiment.

shown in figure 20(*b*). Here, R is the radius of the dipole and (r, θ) are polar coordinates at rest relative to the centre of the dipole. For clarity the positions of only four tracer particles are plotted. One can see that ambient fluid enters the vortex dipole, forming two typical spirals.

In order to explain the results shown in figure 20(*b*), we used a simple kinematic model similar to that proposed by Turner (1964*a*) for spherical thermals. The basic assumption is that at any instant of time the motion inside the vortex dipole is similar to the steady inviscid flow induced by two vortices, while the outside flow is the potential flow around a cylinder. For this model the external (ψ_e) and internal (ψ_i) stream functions are

$$\psi_e = -\bar{U}(r - R^2/r)\sin\theta, \quad r > R, \tag{3.8}$$

$$\psi_i = -\frac{2\bar{U}RJ_1(ar/R)}{aJ_0(a)}\sin\theta, \quad r < R, \tag{3.9}$$

where $\bar{U}$ is the dipole velocity in the direction $\theta = 0$ and $a = 3.83\ldots$ is the first zero of the Bessel function J_1. The stream function ψ_i describes a flow with vorticity distribution $\omega = (a/R)^2\psi_i$ (Batchelor 1967).

The dimensional analysis (see above) and the experimental results (see figure 17) demonstrate that $R(t) = (\frac{1}{2}\alpha)\,\bar{x}(t)$ and hence $\bar{U} = \mathrm{d}\bar{x}/\mathrm{d}t = (2/\alpha)\,\mathrm{d}R/\mathrm{d}t$ ($\alpha = 0.46$). In the coordinate system ($\eta = r/R$, θ) the particle velocities for a flow with the stream functions (3.8), (3.9) are

$$\left.\begin{aligned} \frac{\mathrm{d}\eta}{\mathrm{d}t} &= -\frac{2}{3\alpha t}\left[\tfrac{1}{2}\alpha\eta + \left(1-\frac{1}{\eta^2}\right)\cos\theta\right], \\ \frac{\mathrm{d}\theta}{\mathrm{d}t} &= \frac{2}{3\alpha t\eta}\left(1+\frac{1}{\eta^2}\right)\sin\theta, \end{aligned}\right\} \quad \eta > 1, \tag{3.10}$$

$$\left.\begin{aligned} \frac{\mathrm{d}\eta}{\mathrm{d}t} &= -\frac{2}{3\alpha t}\left[\tfrac{1}{2}2\eta + \frac{2J_1(a\eta)}{J_0(a)\,\eta}\cos\theta\right], \\ \frac{\mathrm{d}\theta}{\mathrm{d}t} &= \frac{2}{3\alpha t\eta}\frac{J_1(a\eta)}{J_0(a)}\sin\theta, \end{aligned}\right\} \quad \eta < 1. \tag{3.11}$$

These equations were integrated numerically. The initial values for t_0, η_0, θ_0 were the same as those in the experiment with the tracer particles. For comparison, the calculated trajectories of four particles, corresponding to the experimental trajectories of four polystyrol spheres in figure 20(*b*), are shown in figure 20(*a*). The stagnation points are marked by crosses. The qualitative agreement is quite satisfactory and the model describes correctly the main feature of the flow, its spiral character.

4. Conclusions

Summarizing the results presented above we can say that localized action of a horizontal force on a stratified fluid produces two typical flows: starting jets and impulsive vortex dipoles. Both of these flows develop in self-similar regimes and their lengthscales increase with time as $t^{\frac{1}{3}}$ and $t^{\frac{1}{5}}$ respectively. The characteristics of the flows depend mainly on one governing parameter: for starting jets it is the non-dimensional force J and for impulsive vortex dipoles it is the kinematic momentum P exerted on the fluid. An interesting feature of the flows considered is that the Richardson number increases with distance $\overline{Ri} \sim \bar{x}^4$ and a buoyancy force rapidly overcomes the inertia force. This reflects the fact that the flow velocity decreases and its vertical dimension increases (steady and starting jets) or remains constant (impulsive dipole) with distance. For comparison, note that gravity-current-type intrusions, by contrast, travel at a constant Richardson number (Simpson 1987).

The next natural step in our studies is the investigation of more complicated vortex structures, which appear as a result of vortex dipole interactions with each other and with a vertical barrier. At present we are continuing our preliminary experiments (Afanasyev *et al.* 1988) and two papers on this fascinating topic have been prepared (Voropayev 1990; Voropayev & Afanasyev 1991).

It is a pleasure to thank Professor G. I. Barenblatt, for numerous helpful discussions on this subject and Dr M. H. Rozovskii for assistance with performing the numerical calculations. Our thanks are also due to Mr I. V. Kat'kov for assistance with photography.

REFERENCES

ABRAMOVICH, S. & SOLAN, A. 1973 The initial development of a submerged laminar round jet. *J. Fluid Mech.* **59**, 791–801.

AFANASYEV, YA, D. & VOROPAYEV, S. I. 1989 On the spiral structure of the mushroom-like currents in the ocean. *Dokl. Akad. Nauk SSSR* **308**, 179–183.

AFANASYEV, YA, D., VOROPAYEV, S. I. & FILIPPOV, I. A. 1988 Laboratory investigation of flat vortex structures in a stratified fluid. *Dokl. Akad. Nauk SSSR* **300**, 704–707.

AFANASYEV, YA, D., VOROPAYEV, S. I. & FILIPPOV, I. A. 1990 Conductivity microprobe for fine structure measurements in stratified flows. *Okeanologiya* **30**, 502–504.

AHLNÄS, K., ROYER, T. C. & GEORGE, T. H. 1987 Multiple dipole eddies in the Alaska coastal current. *J. Geophys. Res.* **92**, 41–47.

BAKER, D. T. 1966 A technique for the precise measurements of small fluid velocities. *J. Fluid Mech.* **26**, 573–575.

BARENBLATT, G. I. 1979 *Similarity, Self-Similarity and Intermediate Asymptotics.* New York: Consultant Bureau.

BATCHELOR, G. K. 1967 *An Introduction to Fluid Dynamics.* Cambridge University Press.

CANTWELL, B. J. 1986 Viscous starting jets. *J. Fluid Mech.* **173**, 159–189.

COUDER, Y. & BASDEVANT, C. 1986 Experimental and numerical study of vortex couples in two-dimensional flows. *J. Fluid Mech.* **173**, 225–251.

ESCUDIER, M. P. & MAXWORTHY, T. 1973 On the motion of turbulent thermals. *J. Fluid Mech.* **61**, 541–552.

FLIERL, G. R., STERN, M. E. & WHITEHEAD, J. A. 1983 The physical significance of modons: Laboratory experiments and general integral constraints. *Dyn. Atmos. Oceans* **7**, 233–263.

GÄRTNER, V. 1983 Visualization of particle displacement and flow in a stratified salt water. *Exps Fluids* **1**, 55–56.

GINSBURG, A. I. & FEDOROV, K. N. 1984 The evolution of a mushroom-formed current in the ocean. *Dokl. Akad. Nauk SSSR* **274**, 481–484.

HEIJST, G. J. F. VAN 1989 Experiments on coherent structures in two-dimensional turbulence. In *Proc. 5th European Phys. Soc. Liquid State Conf. on Turbulence*, pp. 110–111. Moscow, Inst. for Problems in Mech., USSR Acad. Sci.

HEIJST, G. J. F. VAN & FLOR, J. B. 1989 Laboratory experiments on dipole structures in a stratified fluid. Mesoscale/Synoptic coherent structures in geophysical turbulence. In *Proc. 20th Intl Liege Colloqu. on Ocean Hydrodynamics.* Oceanography Series, vol. 50, pp. 591–608. Elsevier.

LAMB, H. 1932 *Hydrodynamics*, 6th edn. Cambridge University Press.

LANDAU, L. D. 1944 New exact solution of Navier–Stokes equations. *Rep. USSR Acad. Sci.* **43**, 286–288.

MCWILLIAMS, J. C. 1983 Interaction of isolated vortices II. *Geophys. Astrophys. Fluid Dyn.* **24**, 1–22.

MCWILLIAMS, J. C. 1984 The emergence of isolated coherent vortices in turbulent flow. *J. Fluid Mech.* **146**, 21–43.

MCWILLIAMS, J. C. & ZABUSKY, J. N. 1982 Interactions of isolated vortices I. *Geophys. Astrophys. Fluid Dyn.* **19**, 207–227.

NGUYEN DUC, J.-M. & SOMMERIA, J. 1988 Experimental characterization of steady two-dimensional vortex couples. *J. Fluid Mech.* **192**, 175–192.

PAPALIOU, D. D. 1985 Magneto-fluid mechanic turbulent vortex street. In *4th Beer-Sheva Seminar on MHD flows and turbulence.* AIAA Progress series, vol. 100, pp. 152–173.

SCHLICHTING, H. 1955 *Boundary Layer Theory.* McGraw-Hill.

SIMPSON, J. E. 1987 *Gravity Currents: In the Environment and the Laboratory.* Ellis Horwood.

SLEZKIN, N. A. 1934 On the case when the equations of motion for viscous fluid can be integrated. *Sci. Papers Moscow State Univ.* **2**, 115–121.

SQUIRE, H. B. 1951 The round laminar jet. *Q. J. Mech. Appl. Maths* **4**, 321–329.

STERN, M. E. & VOROPAYEV, S. I. 1984 Formation of vorticity fronts in shear flow. *Phys. Fluids* **27**, 848–855.

TURNER, J. S. 1964*a* The flow into an expanding spherical vortex. *J. Fluid Mech.* **18**, 195–208.

TURNER, J. S. 1964*b* The dynamics of spheroidal masses of buoyant fluid. *J. Fluid Mech.* **19**, 481–490.

TURNER, J. S. 1986 Turbulent entrainment: the development of the entrainment assumption, and its application to geophysical flows. *J. Fluid Mech.* **173**, 431–471.

VOROPAYEV, S. I. 1983 Free jet and frontogenesis experiments in shear flow. *Tech. Rep., Woods Hole Oceanographic Inst., WHOI*-83-41, pp. 147–159.

VOROPAYEV, S. I. 1985 A theory of self-similar development of a jet in a density homogeneous fluid. *Izv. Akad. Nauk SSSR, Fiz. Atmos. Okeana* **21**, 1290–1294.

VOROPAYEV, S. I. 1987 Modeling of vortex structures in shear flow using a jet of variable impulse. *Morskoy Hydrof. Zh.* **2**, 33–39.

VOROPAYEV, S. I. 1989 Flat vortex structures in a stratified fluid. Mesoscale/Synoptic coherent structures in geophysical turbulence. In *Proc. 20th Intl Liege Colloqu. on Ocean Hydrodynamics.* Oceanography Series, vol. 50, pp. 671–690. Elsevier.

VOROPAYEV, S. I. 1990 Self-similar structures in 2-D turbulence: experimental and theoretical study of vortex multipoles. In *Proc. 3rd European Turbulence Conference, Stockholm, Sweden* (in press).

VOROPAYEV, S. I. & AFANASYEV, YA, D. 1991 Two-dimensional vortex dipole interactions in a stratified fluid. *J. Fluid Mech.* (submitted).

VOROPAYEV, S. I. & FILIPPOV, I. A. 1985 Development of a horizontal jet in a homogeneous and stratified fluids: Laboratory experiments. *Izv. Akad. Nauk SSSR, Fiz. Atmos. Okeana*, **21**, 964–972.

VOROPAYEV, S. I., FILIPPOV, I. A. & AFANASYEV, YA, D. 1989 Self-similar coherent structures in 2-D turbulence: vortex dipoles, quadrupoles and other structures. In *Proc. 5th European Phys. Soc. Liquid State Conf. on Turbulence*, Suppl. issue, pp. 22–23. Moscow, Inst. for Problems in Mech., USSR Acad. Sci.

VOROPAYEV, S. I. & NEELOV, I. A. 1991 Laboratory and numerical modeling of vortex dipoles (mushroom-like currents) in a stratified fluid. *Okeanologiya* **31**, 68–75.